



This discussion paper is/has been under review for the journal *Atmospheric Chemistry and Physics (ACP)*. Please refer to the corresponding final paper in *ACP* if available.

The accuracy of the
RTTOV fast radiative
transfer model

M. Matricardi

An assessment of the accuracy of the RTTOV fast radiative transfer model using IASI data

M. Matricardi

ECMWF, Shinfield Park, Reading, Berkshire, RG2 9AX, UK

Received: 25 February 2009 – Accepted: 1 April 2009 – Published: 14 April 2009

Correspondence to: M. Matricardi (marco.matricardi@ecmwf.int)

Published by Copernicus Publications on behalf of the European Geosciences Union.

| | |
|--|------------------------------|
| Title Page | |
| Abstract | Introduction |
| Conclusions | References |
| Tables | Figures |
| ◀ | ▶ |
| ◀ | ▶ |
| Back | Close |
| Full Screen / Esc | |
| Printer-friendly Version | |
| Interactive Discussion | |

Abstract

IASI measurements of spectral radiances made between the 1 April 2008 and the 15 April 2008 are compared with simulations performed using the RTTOV fast radiative transfer model utilizing regression coefficients based on different line-by-line models. The comparisons are performed within the framework of the European Centre for Medium-Range Weather Forecasts Integrated Forecasting System using fields of temperature, water vapour and ozone obtained from short-range forecasts. Simulations are performed to assess the accuracy of the RTTOV computations and investigate relative differences between the line-by-line models and the quality of the spectroscopic databases on which the RTTOV coefficients are based.

1 Introduction

The exploitation of satellite radiance data for Numerical Weather Prediction (NWP) requires the use of an accurate and fast radiative transfer (RT) model to simulate radiances from an input atmospheric profile. The high spectral resolution of radiances measured by the Atmospheric Infrared Sounder (AIRS) (Aumann et al., 2003) on the Earth Observing System (EOS) Aqua platform and the Infrared Atmospheric Sounding Interferometer (IASI) (Chalon et al., 2001) on the MetOp-A platform provides temperature and constituent profiles at a higher accuracy and with more vertical resolution than the conventional filter wheel radiometers. The assimilation of AIRS and IASI long-wave temperature sounding channels at ECMWF has produced a significant positive impact on forecast quality (McNally et al., 2006; Collard and McNally, 2008) and in the near future the use of IASI data could be extended to other spectral bands. The variational approach to the assimilation of these datasets into the ECMWF four-dimensional variational analysis scheme, 4D-Var (Rabier et al., 1998), involves the definition of the observation-error covariance matrix that is used to specify errors associated with radiance data. The observation-error covariance matrix is the sum of the instrumental-error

ACPD

9, 9491–9535, 2009

The accuracy of the RTTOV fast radiative transfer model

M. Matricardi

[Title Page](#)

[Abstract](#)

[Introduction](#)

[Conclusions](#)

[References](#)

[Tables](#)

[Figures](#)

◀

▶

◀

▶

[Back](#)

[Close](#)

[Full Screen / Esc](#)

[Printer-friendly Version](#)

[Interactive Discussion](#)



covariance matrix and the forward-model-error covariance matrix which is based on the estimation of errors associated with fast RT models. The low noise level of IASI and AIRS makes RT errors an important contribution to the definition of the observation-error covariance matrix and consequently they must be properly evaluated and their origin fully understood.

Fast RT model errors are dominated by two main components: the parameterization used for the atmospheric transmittances and the errors associated with the spectroscopic parameters and the computational procedures adopted in the line-by-line (LBL) models on which fast RT models are generally based. The fast RT model used operationally at the European Centre for Medium-Range Weather Forecasts (ECMWF) is the Radiative Transfer Model for TOVS (RTTOV) (Saunders et al., 1999). In RTTOV the transmittances of the atmospheric gases are expressed as a function of profile-dependent predictors. This parameterization of the transmittances makes the model computationally efficient and thus fulfils the NWP requirement of near real-time monitoring and assimilation of satellite radiance data. In fact, LBL models are too computationally expensive to be used in an NWP operational environment. In this paper we give a brief review of the current status of the RTTOV model and discuss the main features of the LBL models that have been used to derive the RTTOV coefficients for IASI focusing on the aspects that distinguish one model from another.

Errors associated to the RTTOV transmittance parameterization for the IASI channels are discussed in detail in Matricardi (2008) whereas LBL model errors have been investigated in several studies (e.g., Rizzi et al. 2002; Tjemkes et al., 2003) using high-spectral resolution aircraft data. In this paper we try to assess the absolute accuracy of the RTTOV model as a whole. The availability of RTTOV regression coefficients based on different LBL models has also offered the opportunity to investigate relative differences between LBL-models and the quality of the spectroscopic databases used in the LBL-model computations. The assessment of the RTTOV accuracy has been carried out by running a number of Integrated Forecast System (IFS) monitoring experiments where IASI spectra simulated by RTTOV have been compared to IASI spectra

The accuracy of the RTTOV fast radiative transfer model

M. Matricardi

[Title Page](#)

[Abstract](#)

[Introduction](#)

[Conclusions](#)

[References](#)

[Tables](#)

[Figures](#)

◀

▶

◀

▶

[Back](#)

[Close](#)

[Full Screen / Esc](#)

[Printer-friendly Version](#)

[Interactive Discussion](#)



measured during the period 1–15 April 2008 using short range operational forecasts of temperature, water vapour and ozone fields to specify the RTTOV input state vector.

2 The RTTOV model

The RTTOV model was originally developed at ECMWF (Eyre and Woolf, 1988) to retrieve temperature and humidity profiles from the Television InfraRed Observation Satellite (TIROS-N) Operational Vertical Sounder (TOVS) (Smith et al., 1979). Subsequently the code has gone through several developments (e.g., Matricardi et al., 2004), more recently within the EUMETSAT NWP Satellite Application Facility (SAF), of which RTTOV-9 is the latest version (Saunders et al., 2008). RTTOV covers the spectral range 3–20 microns in the infrared and the frequency range 10–200 GHz in the microwave and supports a large number of platforms and sensors with updates as new sensors are launched. An important feature of the RTTOV model that is essential for use in a NWP environment is that it not only performs the fast computation of the forward (or direct) radiances but also the fast computation of the gradient of the radiances with respect to the state vector variables for the input state vector values (i.e. temperature, variable gas concentrations, cloud and surface properties).

The model uses the polychromatic form of the radiative transfer equation (i.e. the use of channel averaged transmittances in the radiative transfer equation is based on the assumption that this is equivalent to the convolution of the monochromatic radiances) (see Matricardi et al., 2004, for details). The polychromatic approximation is adequate when channels are narrow enough that the convolution of the Planck function can be replaced with its value at the central wave number of the channel. For IASI and AIRS channels the polychromatic approximation results in errors typically below 0.05 K whereas for broad channels the accuracy is generally poor and can result in biases of \sim 1–2 K (Brunel and Turner, 2003). The RTTOV fast transmittance scheme uses regression coefficients derived from accurate LBL computations to express the optical depths as a linear combination of profile dependent predictors that

The accuracy of the RTTOV fast radiative transfer model

M. Matricardi

[Title Page](#)

[Abstract](#)

[Introduction](#)

[Conclusions](#)

[References](#)

[Tables](#)

[Figures](#)

[◀](#)

[▶](#)

[◀](#)

[▶](#)

[Back](#)

[Close](#)

[Full Screen / Esc](#)

[Printer-friendly Version](#)

[Interactive Discussion](#)



are functions of temperature, absorber amount, pressure and viewing angle (Matricardi and Saunders, 1999). The regression coefficients are computed using a training set of diverse atmospheric profiles chosen to represent the range of variations in temperature and absorber amount found in the atmosphere. Regression coefficients for 5 RTTOV are available based on the 43 profile training set described in Matricardi and Saunders (1999), the 52 profile training set described in Chevallier (2000) and, more recently, on the 83 profile training set described in Matricardi (2008) (henceforth we will refer to these training sets as ECMWF_43_P, ECMWF_52_P and ECMWF_83_P, respectively). The latter dataset includes variable profiles of carbon dioxide (CO_2), nitrous 10 oxide (N_2O), methane (CH_4) and carbon monoxide (CO) in addition to water vapour (H_2O) and ozone (O_3). The LBL computations for the minor gases that are not allowed to vary in RTTOV are carried out assuming a climatological mean profile (see next 15 section for details).

The RTTOV-9 fast transmittance algorithm supports a range of predictor sets, namely 15 RTTOV-7 predictors, RTTOV-8 predictors and RTTOV-9 predictors. The selection of the predictors is made according to the coefficients file supplied to the program. The RTTOV-8 predictors (Matricardi et al., 2004) allow to vary the amounts of H_2O , O_3 and optionally CO_2 whereas the RTTOV-9 predictors (Matricardi, 2003) allow to vary the amounts of H_2O , O_3 , CO_2 , N_2O , CH_4 and CO. Coefficients based on RTTOV-9 20 predictors can only be used for AIRS and IASI and input profiles for CO_2 , N_2O , CH_4 and CO are mandatory. In addition, RTTOV-9 predictors can be used to compute optical depths for the long atmospheric paths involved in the computation of top of the atmosphere (TOA) radiances if solar radiation is required to be included in the short-wave infrared channels.

Regression coefficients are computed separately for all gases with fixed amounts 25 and for each species that is allowed to vary. Since the convolution of the transmittance of all the gases differs from the product of the transmittance of the single gases convolved individually, effective transmittances are derived that allow Beer's law to be obeyed to a very good approximation (Matricardi and Saunders, 1999). The accuracy

The accuracy of the RTTOV fast radiative transfer model

M. Matricardi

[Title Page](#)

[Abstract](#)

[Introduction](#)

[Conclusions](#)

[References](#)

[Tables](#)

[Figures](#)

◀

▶

◀

▶

[Back](#)

[Close](#)

[Full Screen / Esc](#)

[Printer-friendly Version](#)

[Interactive Discussion](#)



of the fast model transmittance parameterization can be assessed by comparing the transmittances and radiances computed by the fast model with the corresponding values from LBL models in different ways. Firstly, the fast model transmittance profiles and TOA radiances computed for the regression training data set can be compared with LBL model equivalents to determine the accuracy of the fast model itself. Secondly, a set of profiles independent of the regression coefficients can be used to allow uncertainties from different type of profiles to be included. The accuracy of the RTTOV-9 predictors is discussed in detail in Matricardi (2008). Results for an independent profile set show that the root mean square (rms) of the difference between fast model and LBL radiances is below 0.15 K for the vast majority of the channels. Larger errors are observed in spectral regions that see the presence of medium strength water vapour lines, in the ozone band at 9.8 microns and in regions where H₂O lines interfere with absorption lines of other gas species. Results for RTTOV-8 predictors are similar (Matricardi et al., 2004). If we use this error figure as representative of errors associated with the RTTOV fast transmittance parameterization then we can reasonably assume that the RTTOV accuracy is largely determined by the accuracy of the LBL algorithm. For instance the inaccurate knowledge of molecular line strengths alone can result in TOA radiance errors as large as 0.3–0.4 K (Rizzi et al., 2002).

The computation of TOA radiances in RTTOV-9 is performed using a parameterization of the Planck function based on the linear-in- τ assumption that the source function throughout an atmospheric layer is linear with the optical depth, τ , of the layer. An altitude dependent correction to the local path is also applied that takes into account the curvature of the Earth and its surrounding atmosphere. Finally, to compute the infrared emissivity over water a fast surface emissivity routine, ISEM, (Sherlock, 1999) is used.

The accuracy of the RTTOV fast radiative transfer model

M. Matricardi

[Title Page](#)

[Abstract](#)

[Introduction](#)

[Conclusions](#)

[References](#)

[Tables](#)

[Figures](#)

◀

▶

◀

▶

[Back](#)

[Close](#)

[Full Screen / Esc](#)

[Printer-friendly Version](#)

[Interactive Discussion](#)



3 The line-by-line models

ACPD

9, 9491–9535, 2009

- As discussed in the previous section, the RTTOV fast transmittance algorithm uses regression coefficients obtained from LBL transmittance calculations. As noted in Rizzi et al. (2002), LBL model errors tend to be dominated by insufficient knowledge of basic spectroscopy rather than by the computational procedures used in the codes. Spectroscopic errors are of paramount importance for high-resolution sounders like AIRS and IASI that allow the use of channels placed between spectral lines. These channels have weighting functions that are sharper than the weighting functions that characterize the channels placed on top of the spectral lines and consequently particular attention must be paid to the spectral line shape of species like H_2O and CO_2 for which optical depths in the atmosphere can reach very large values. The effect of line mixing, i.e. the change in line shape due to the redistribution of radiation in overlapping spectral lines (Strömgren and Reuter, 1988), in the CO_2 Q-branches is now routinely incorporated in LBL algorithms and in the recent past progress has been made in the development of improved CO_2 line shapes by taking into account the effect of line mixing in CO_2 P/R-branches (e.g. Niro et al., 2005). Progress in the development of improved H_2O line shapes is still hindered by the difficulty of achieving good measurements of H_2O amounts in the atmosphere and in the laboratory and the nature of water vapour continuum absorption and its effect on atmospheric radiance is an outstanding and unresolved issue (e.g. Ma et al., 2008). In LBL models water vapour continuum is usually parameterized using the semi-empirical CKD model by Clough et al. (1989). This model has been recently revised (Tobin et al., 1999) based on the assumption that the continuum absorption in water vapour bands is dominated by the collision-induced absorption resulting from the generation of a short-lived complex of water vapour and colliding molecules (MT_CKD model). Finally, the accuracy of the line parameters used in the LBL calculations can introduce significant errors in the simulated radiances (Tjemkes et al., 2003).

RTTOV regression coefficients for IASI are available based on various LBL models.

The accuracy of the RTTOV fast radiative transfer model

M. Matricardi

[Title Page](#)

[Abstract](#)

[Introduction](#)

[Conclusions](#)

[References](#)

[Tables](#)

[Figures](#)

◀

▶

◀

▶

[Back](#)

[Close](#)

[Full Screen / Esc](#)

[Printer-friendly Version](#)

[Interactive Discussion](#)



Regression coefficients based on version 4 of the GENLN2 LBL model (GENLN2_v4) and version 11.1 of the LBLRTM LBL model (LBLRTM.v11.1) have been generated at ECMWF using RTTOV-9 predictors whereas coefficients based on version 1.11 of the kCARTA LBL model (kCARTA_v1.11) have been generated at Meteo France using

5 RTTOV_8 predictors. A description of the LBL models is given in the following sections.

3.1 GENLN2_v4

GENLN2_v4 (Edwards, 1992) is a line-by-line atmospheric transmittance and radiance model. Line strengths and half-widths are adjusted to the path pressure and temperature and Doppler broadening of the spectral lines is taken into account. To describe

10 the effects of pressure and Doppler line broadening, GENLN2_v4 adopts the Voigt line shape. The GENLN2_v4 CO₂ line shape includes the effect of line mixing and takes into account the sub-Lorentzian behaviour in the far-wing of the line. If data is available, CO₂ Q-branch line mixing in the ν_2 and ν_3 band can be included out to an arbitrary 10 cm⁻¹ from line centre. For greater distances from the centre the line shape

15 is approximated by the empirical model by Cousin et al. (1985). This model explains the sub-Lorentzian nature of the CO₂ far wing line shape in terms of duration of collision effects and uses a temperature dependent χ -factor to adjust the standard line shape function based on the impact theory. If no line-mixing data is available then the sub-Lorentzian line shape is used everywhere. The standard release of GENLN2_v4

20 includes the water vapor continuum model CKD_2.1. However, we carried out our computations using the model CKD_2.4 that became available at the time the regression coefficients were about to be generated. The pressure-broadened band of N₂ at 2350 cm⁻¹ (Menoux et al., 1993) and that of O₂ at 1550 cm⁻¹ (Timofeyev and Tonkov,

1978; Rinsland et al., 1989) is included as broadband continuum contribution to the absorption and heavy molecules can be modeled using high-resolution cross-sectional data. In our computations, CO₂Q-branch line mixing has been fully accounted for using first order line-mixing coefficients from Strow et al. (1994).

The accuracy of the RTTOV fast radiative transfer model

M. Matricardi

[Title Page](#)

[Abstract](#)

[Introduction](#)

[Conclusions](#)

[References](#)

[Tables](#)

[Figures](#)

◀

▶

◀

▶

[Back](#)

[Close](#)

[Full Screen / Esc](#)

[Printer-friendly Version](#)

[Interactive Discussion](#)



3.2 kCARTA_v1.11

The kCARTA_v11.1 model (De Souza-Machado et al., 2002) is a fast LBL algorithm where transmittances are computed from compressed look-up tables of atmospheric transmittances (Strow et al., 1998). The look-up tables are computed using a LBL model developed at the University of Maryland, Baltimore County (UMBC-LBL) (Strow et al., 2003) and their use in kCARTA results in very fast computation times. The water vapour continuum model (hence after referred to as MTK_CKD_UMBC) is based on the MTK_CKD_1.0 model. It uses revised values of the spectral density function coefficients based on measurements of AIRS spectra utilizing in-situ data available from the ARM sites (De Souza-Machado, personal communication, 2008). Line mixing coefficients for CO₂ are available for 12 P/R-branch bands and 12 Q-branch bands in the short wave and in the long wave. The kCARTA model for the CO₂ line shape is based on the work by Tobin (1996) and De Souza-Machado et al. (1999). For the P/R-branch it involves an approximation for the combination of line mixing and duration-of-collision effects. Regarding the UMBC-LBL model it should be stressed that it relies on a full treatment of the CO₂ Q- and P/R-branch line mixing and does not use the perturbation theory. Finally, the collision-induced bands of oxygen at 1600 cm⁻¹ and nitrogen at 2350 cm⁻¹ are incorporated using the model by Thibault et al. (1997) and Lafferty et al. (1996), respectively.

20 3.3 LBLRTM_v11.1

The LBLRTM line-by-line model (Clough et al., 1992) has been developed at the Atmospheric and Environmental Research Inc. (AER). To describe the effects of pressure and Doppler line broadening the Voigt line shape is used at all atmospheric levels with an algorithm based on a linear combination of approximating functions. LBLRTM incorporates the self- and foreign-broadened water vapor continuum model MT_CKD_2.0 (Tobin et al., 1999) and the collision-induced bands of oxygen at 1600 cm⁻¹ and nitrogen at 2350 cm⁻¹ are included as broad-band continuum contributions to the absorp-

The accuracy of the RTTOV fast radiative transfer model

M. Matricardi

[Title Page](#)

[Abstract](#)

[Introduction](#)

[Conclusions](#)

[References](#)

[Tables](#)

[Figures](#)

◀

▶

◀

▶

[Back](#)

[Close](#)

[Full Screen / Esc](#)

[Printer-friendly Version](#)

[Interactive Discussion](#)



tion using the models by Thibault et al. (1997) and Lafferty et al. (1996), respectively. In LBLRTM the CO₂ line shape includes the effects of line mixing for the P-R-branch and Q-branch in the ν_2 and ν_3 band using first order line coupling parameters generated using the code by Niro et al., 2005. Since the model by Niro et al. (2005) combines the
5 effects of line mixing and duration of collision effects, the χ factor is set equal to 1. In addition, the CO₂ continuum is computed using the Niro et al. (2005) coupling coefficients with a scaling factor of 0.75 applied to the ν_3 -band to agree with AIRS spectra in the ν_3 spectral region. LBLRTM uses temperature dependent cross section data to model the absorption of heavy molecules. The pressure dependence of the cross
10 sections is treated by performing a convolution of the cross section spectrum with an appropriate Lorentz function.

The computation of the LBL transmittances is performed on a grid of vertical levels of fixed pressure for a regression dataset of diverse atmospheric profiles and require the use of appropriate parameters from a molecular database. These details are summarized in Table 1. Note how for kCARTA and GENLN2 the same molecular database
15 has been used although it should be noted that for GENLN2 the use of the Strow et al. (1994) line mixing coefficients requires the use of CO₂ molecular line parameters from the HITRAN_1992 compilation. For the LBLRTM computations we have envisaged a molecular database that blends line parameters obtained from various
20 sources. This is based on the results shown in Matricardi (2007) which suggest that in a number of spectral regions the use of line parameters from different sources can result in a better agreement of simulations with observations. This blended database is largely drawn from HITRAN_2004 (Rothman et al., 2005) and includes updates up
25 to 1 January 2007. However, in the 9.8 micron ozone band we use ozone line parameters from HITRAN_2000 (Rothman et al., 2003) whereas in the spectral region between 1700 and 2400 cm⁻¹ we use water vapour line parameters from GEISA_2003 (Jaquinot-Husson et al., 2005). Although Matricardi (2007) suggests that the use of CO₂ line parameters from GEISA_2003 could also be envisaged in the 15 micron CO₂ band, the use of Niro et al. (2005) line mixing coefficients requires that line parameters

The accuracy of the RTTOV fast radiative transfer model

M. Matricardi

[Title Page](#)

[Abstract](#)

[Introduction](#)

[Conclusions](#)

[References](#)

[Tables](#)

[Figures](#)

◀

▶

◀

▶

[Back](#)

[Close](#)

[Full Screen / Esc](#)

[Printer-friendly Version](#)

[Interactive Discussion](#)



for CO₂ are obtained from the HITRAN_2000 compilation. From Table 1 it can also be seen that regression coefficients are based on different profile training sets and that all the computations have been performed on the 101 level vertical grid specified by the AIRS science team (Strøm et al., 2003).

For the interpretation of the results we find it useful to include two figures where differences between the various water vapour continuum models are illustrated. In particular, in Fig. 1 we show the water vapour broadening coefficients for the self continuum while in Fig. 2 we show the broadening coefficients for the foreign continuum (self broadening due to H₂O-H₂O collisions is the dominant source of continuum in the window regions whereas foreign broadening due H₂O-N₂ collisions dominates in the water vapour band). These figures show that in the 10 micron window region MTK_CKD UMBC self broadening coefficients are smaller than CKD_2.4 and MTK_CKD_v1.4 coefficients. In the centre of the water vapour band around 1600 cm⁻¹ the CKD_2.4 foreign broadening coefficients are smaller than MTK_CKD UMBC and MTK_CKD_v1.4 coefficients whereas for larger wave numbers MTK_CKD UMBC foreign broadening coefficients are larger than CKD_2.4 and MTK_CKD_v1.4 coefficients.

All LBL datasets include N₂, O₂, HNO₃, OCS, CCl₄, CF₄, CCl₃F and CCl₂F₂ among the gases with fixed amount. Regression coefficients based on the GENLN2 and LBLRTM models allow the variation of CO₂, N₂O, CO, and CH₄ amounts whereas in kCARTA the amount of these gas species is fixed. The LBLRTM dataset includes an additional number of fixed gas species, i.e. NO₂, SO₂ and NO. In general, atmospheric constituent profiles for all gases are based on AFGL profiles scaled to reflect present-day concentrations. However, in the LBLRTM dataset we have used HNO₃ and NO profiles generated using the MOZART chemical transport model (Hauglustaine et al., 1998) whereas in the kCARTA dataset the concentrations of CO₂, N₂O, CO and CH₄ are based on the climatological profiles described in Matricardi (2003).

The accuracy of the RTTOV fast radiative transfer model

M. Matricardi

[Title Page](#)

[Abstract](#)

[Introduction](#)

[Conclusions](#)

[References](#)

[Tables](#)

[Figures](#)

◀

▶

◀

▶

[Back](#)

[Close](#)

[Full Screen / Esc](#)

[Printer-friendly Version](#)

[Interactive Discussion](#)



4 The monitoring experiments

Three baseline monitoring experiments have been run using cycle 33 R1 of the IFS (which was the operational cycle from June until October 2008) using the T799 horizontal truncation. This truncation corresponds to a horizontal resolution of ~ 25 km. A feature of cycle 33 R1 of the IFS is a vertical discretization of the atmosphere into a grid of 91 pressure levels. The model uses a hybrid vertical coordinate with coordinates that follow the orography of the terrain in the lower troposphere and pressure coordinates in the stratosphere above about 60 hPa. The top level is fixed at 0.01 hPa (about 80 km) and of the 91 levels in the vertical, 52 are above 100 hPa. The state vector variables used in the RTTOV simulations are forecast fields of temperature, humidity, ozone and surface parameters. IASI data within a 12-h 4D-VAR window are grouped into 30 min time slots. A T799 high resolution forecast is then run from the previous analysis and observation minus model differences are computed for IASI soundings within a given time slot. This sequence is then repeated for each 12-h 4D-VAR window. In this study we consider IASI data inside 12-h 4D-VAR windows during the period 1–15 April 2008. The statistics of the difference between global radiosonde observations and ECMWF analyses in the troposphere show values of the standard deviation typically between 0.5 K and 1 K for temperature and between 0.5 and 1.5 g/Kg for water vapour. In the stratosphere, standard deviations for temperature can reach 1.5 K. Ancillary data used in the RTTOV computations include sea-surface temperature (SST). SST fields in cycle 33 R1 are based on analyses received from the National Centers for Environmental Prediction (NCEP), Washington, DC, on a $0.5^\circ \times 0.5^\circ$ grid. These analyses are based on ship, buoy and satellite observations. The SST root mean square error (rms) relative to buoy observations is ~ 0.36 K (Kara et al., 2007). However, this figure can be significantly different in shallow waters where rapid changes due to the upwelling radiation can occur close to land.

Since the the RTTOV optical depth computations are defined by the number of levels in the coefficient file, the IFS pressure levels must be interpolated to the same levels as

The accuracy of the RTTOV fast radiative transfer model

M. Matricardi

[Title Page](#)

[Abstract](#)

[Introduction](#)

[Conclusions](#)

[References](#)

[Tables](#)

[Figures](#)

◀

▶

◀

▶

[Back](#)

[Close](#)

[Full Screen / Esc](#)

[Printer-friendly Version](#)

[Interactive Discussion](#)



the coefficient files. To this end we have used the RTTOV-9 new internal interpolation scheme that allows the input profile to be defined by the user. However, it should be noted that although RTTOV computes optical depths on the levels specified in the coefficient files, the integration of the RT equation is performed on the 91 IFS levels.

- 5 To ensure that the Jacobians are properly mapped back on the user levels, the optical depths must be interpolated to the IFS levels using the same interpolation scheme utilized for the atmospheric variables.

The IASI spectra used in our experiments are measured over the sea. To reduce the amount of data we have sub-sampled by arbitrarily selecting one out of eleven scan-
10 positions. This also ensures that for two adjacent scan lines we always sample two different scan positions. Only channels detected as clear by the ECMWF cloud detection algorithm are processed. Since the ECMWF cloud detection algorithm (McNally and Watts, 2003) finds clear channels rather than clear locations, the size of sample varies with the sensitivity of the channel to clouds. Channels characterized by weight-
15 ing functions that peak at high altitudes are less sensitive to clouds than channels with weighting functions that peak at low altitudes or at the surface. To illustrate this, in Fig. 3 we show the size of the sample for each channel in three latitude bands. It can be clearly seen that the size of the sample varies from several thousands spectra for the channels peaking at middle and high altitudes to a few thousands for channels
20 peaking at low altitudes or at surface. To avoid reflected solar radiation and non-LTE effects (the latter are not modelled in RTTOV), in the spectral region between 2000 and 2760 cm^{-1} we have sampled only night-time spectra. This is reflected in Fig. 3 where the size of the sample in this spectral region is significantly smaller than the size of the sample in other spectral regions. Note that to exclude night-time spectra
25 we have used the criterium that the local solar zenith angle is greater than 100° . This means that a given location can be considered not to be in daylight up to an altitude of $\sim 100\text{ km}$ (i.e. the altitude above which we consider the atmosphere to be transparent in our calculations).

In our RTTOV computations the state vector includes profiles of temperature, water

The accuracy of the RTTOV fast radiative transfer model

M. Matricardi

[Title Page](#)

[Abstract](#)

[Introduction](#)

[Conclusions](#)

[References](#)

[Tables](#)

[Figures](#)

◀

▶

◀

▶

[Back](#)

[Close](#)

[Full Screen / Esc](#)

[Printer-friendly Version](#)

[Interactive Discussion](#)



vapour and ozone, surface parameters (e.g. skin temperature and surface pressure) and a wave number dependent value of the sea surface emissivity that includes the dependence on the viewing geometry. In addition to the profiles of temperature, water vapour and ozone, the experiments that use RTTOV coefficients based on GENLN2 and LBLRTM also require input profiles of CO₂, CO, N₂O and CH₄. Since profiles for these trace gases are not prognostic variables in the ECMWF model we had to fix the amounts in the GENLN2 and LBLRTM experiments. To this end we have chosen the values assumed in the LBL computation used to train kCARTA. The rationale behind this choice is that at present kCARTA coefficients are used operationally at ECMWF for the assimilation of AIRS and IASI radiances and we want to use the kCARTA spectra as benchmark in our comparisons.

5 Discussion of the results

5.1 IASI band 1 (645 to 1200 cm⁻¹)

Results in IASI band 1 are plotted in Figs. 4, 5, and 6 where we show the mean value of the difference (bias) between observed and simulated radiances in units of equivalent black body brightness temperature for the Northern Hemisphere (30° N–90° N), tropics (30° N–30° S) and Southern Hemisphere (30° S–90° S), respectively. In the top panel the LBLRTM spectrum (solid red line) is superimposed on the kCARTA spectrum (solid black line) whereas in the bottom panel the GENLN2 spectrum (solid red line) is superimposed on the kCARTA spectrum. Results show that for all experiments biases are generally within ±1 K in all geographical regions. The only exception is the ozone band at 9.8 microns where biases can reach 1.5 K in the Northern Hemisphere.

5.1.1 Results in the temperature sounding band

Of particular interest are the result obtained in the 15 microns temperature sounding CO₂v2 band where the GENLN2 experiment shows significantly larger biases between

| | |
|--|------------------------------|
| Title Page | |
| Abstract | Introduction |
| Conclusions | References |
| Tables | Figures |
| ◀ | ▶ |
| ◀ | ▶ |
| Back | Close |
| Full Screen / Esc | |
| Printer-friendly Version | |
| Interactive Discussion | |



700 cm⁻¹ and 750 cm⁻¹. To interpret this result we should bear in mind that, as discussed in Sect. 3, GENLN2 uses the Cousin et al. (1985) empirical model to describe the far-wing shape of the CO₂ line shape. The χ -factor used in the v2-band is based on spectra measured in the v3-band. However, the symmetry of the 4.3 microns bands is different from the symmetry of the 15 microns bands and consequently the component of the χ factor due to line mixing is in error and the effect of line-mixing will be over-estimated in GENLN2. As shown in Figs. 4, 5, and 6, errors in the GENLN2 CO₂ line shape can significantly degrade the accuracy of the spectra.

As discussed above, the performance of GENLN2 between 700 to 750 cm⁻¹ can be explained in terms of the different treatment of the far-wing CO₂ line shape. In the same spectral region kCARTA and LBLRTM spectra show similar features with differences not larger than 0.2 K. However, the kCARTA spectrum is more irregular than the LBLRTM spectrum. This behaviour can be affected by factors that include the line mixing model, uncertainties in the temperature profile and errors in the strengths and widths of the weak water vapour lines originating from the edge of the water vapour pure rotational band. The errors in the line strengths and widths can either be due to uncertainties in the water vapour profile or due to spectroscopic errors (in addition to this kCARTA and LBLRTM use different water vapour molecular databases).

The very close similarities between the LBLRTM and GENLN2 spectra and the differences between these two models and kCARTA in the 645 to 700 cm⁻¹ spectral region can only be explained in terms of the line mixing model used in the LBL models. In fact, these differences cannot be attributed to the molecular parameters since, for instance, LBLRTM and kCARTA use the same HITRAN_2000 compilation. Regarding the absolute value of the biases, it should be noted that in this spectral region a consistent number of channels is sensitive to emission at high altitudes and consequently biases can be affected by systematic temperature errors of the ECMWF model in the upper stratosphere and mesosphere.

A feature in common to the LBLRTM and GENLN2 spectra is the large bias (between 1.8 K and 2 K) seen in correspondence to the CO₂ Q-branch at 667 cm⁻¹. Since

The accuracy of the RTTOV fast radiative transfer model

M. Matricardi

[Title Page](#)

[Abstract](#)

[Introduction](#)

[Conclusions](#)

[References](#)

[Tables](#)

[Figures](#)

[◀](#)

[▶](#)

[◀](#)

[▶](#)

[Back](#)

[Close](#)

[Full Screen / Esc](#)

[Printer-friendly Version](#)

[Interactive Discussion](#)



GENLN2 andLBLRTM use line mixing coefficients based on a 1st order perturbation theory, it would appear that this is not adequate for the 667 cm^{-1} Q-branch.

5.1.2 Results in the ozone sounding band

Spectra in the ozone band are remarkably close. Biases observed in the ozone band
5 are probably dominated by spectroscopic errors although the larger values (up to -1.6 K) observed in the Northern Hemisphere might reflect a poor performance of the ozone assimilation system.

5.1.3 Results in the window regions

The absorption in the window regions between 800 and 1200 cm^{-1} is primarily due
10 to water vapour and consists mainly of the absorption due to water vapour self-continuum although in the high-wavenumber boundary of the window (i.e. between 1080 and 1200 cm^{-1}) the contribution of weak water vapour lines originating in the ν_2 -band has also to be taken into account. With the exception of a few channels, the specification
15 of the continuum model and the choice of the molecular parameters do not appear to have a significant impact on the spectra obtained in the Northern and Southern Hemispheres. In fact, within each of these geographical regions, spectra are very similar with biases varying between -0.1 and -0.6 K in the Northern Hemisphere and between -0.1 and -0.4 K in the Southern Hemisphere.

It is difficult to interpret the differences observed between the biases obtained in
20 the Northern and Southern Hemispheres between 800 and 1000 cm^{-1} . The absorption due to the water vapour self continuum is proportional to the square of the water vapour amount and for a fixed amount of water vapour it decreases with temperature. In general, the colder air masses typically encountered at mid-high latitudes are associated with less water vapour and the competing effect of temperature and water amount
25 is stronger than in the much more humid conditions encountered in the tropical regions. Errors in the temperature profiles and, above all, errors in the water vapour profiles in

[Title Page](#)

[Abstract](#)

[Introduction](#)

[Conclusions](#)

[References](#)

[Tables](#)

[Figures](#)

◀

▶

◀

▶

[Back](#)

[Close](#)

[Full Screen / Esc](#)

[Printer-friendly Version](#)

[Interactive Discussion](#)



the lower troposphere and near the surface can then affect the simulated spectra in various measures and result in the different biases observed at different latitudes.

Biases can also be affected by errors in the SST analysis. In addition, SST errors indirectly affect the values of the sea surface emissivities computed by ISEM since ISEM does not take into account the temperature dependence of the water vapour optical parameters. However, since the SST is used as the skin temperature in the RT computations, the larger biases in the Northern Hemisphere cannot be explained in terms of SST alone since this feature should also be present in the high-wavenumber boundary of the window region. It is also possible that channels identified by the cloud detection scheme as clear channels are in fact channels affected by clouds. The negative sign of the biases (i.e. the RT model overestimates the radiances) is consistent with this hypothesis. However, results obtained using aircraft data in controlled clear-sky conditions (e.g. Rizzi et al., 2002) show biases whose magnitude is similar to that obtained in our study. Consequently, the effect due to errors in the cloud detections scheme must be very small.

Results for the tropical region (Fig. 5) show that in contrast to the cases discussed above, differences now exist between the spectra in the window regions. This is a direct consequence of the fact that the high tropical water vapour column concentrations make the water vapour continuum absorption a much more important factor. We have studied this aspect more in depth by running a further experiment where the kCARTA spectra have been computed using the same water vapour continuum model used in the LBLRTM model. The results are shown Fig. 7 where we have plotted the difference between the standard kCARTA mean spectrum and the LBLRTM mean spectrum (top panel) and the difference between the modified kCARTA mean spectrum and the LBLRTM mean spectrum (bottom panel).

Fig. 7 shows that the use of the same continuum model greatly reduce the differences between the spectra. This is all the more evident between 800 and 980 cm⁻¹. The residuals seen in correspondence of the CFCI₃ band at 846 cm⁻¹ and the CF₂Cl₂ band at 923 cm⁻¹ are attributable to the different amounts used for these molecules

The accuracy of the RTTOV fast radiative transfer model

M. Matricardi

[Title Page](#)

[Abstract](#)

[Introduction](#)

[Conclusions](#)

[References](#)

[Tables](#)

[Figures](#)

◀

▶

◀

▶

[Back](#)

[Close](#)

[Full Screen / Esc](#)

[Printer-friendly Version](#)

[Interactive Discussion](#)



in kCARTA and LBLRTM whereas residuals around 880 cm^{-1} should be attributed to the spectroscopy. In the window region between 1080 and 1200 cm^{-1} the change in the continuum reduces the peak-to-peak differences and shifts the biases towards positive values. This would suggest that in this spectral region differences between the spectra are attributable primarily to differences between the molecular databases. Results shown in the bottom panel of Fig. 7 corroborate this hypothesis in that GENLN2 and kCARTA biases are in very good agreement (they use the same HITRAN_2000 molecular database).

Finally, we want to comment on the feature (a kink) in the GENLN2 spectrum around 1000 cm^{-1} observed in the tropics and in the Southern Hemisphere. This feature is not present in the kCARTA and LBLRTM experiments and its origin is difficult to interpret. In this spectral region, the only obvious difference between GENLN2 and the other LBL models is the much smaller value of the foreign broadening spectral density function but it is difficult to argument in favour of a possible impact of the foreign continuum since foreign broadening should not be important at these wave numbers.

5.2 IASI band 2 (1200 to 2000 cm^{-1})

Spectra in IASI band 2 are plotted in Figs. 8, 9, and 10 for the Northern Hemisphere, tropics and Southern Hemisphere, respectively. The values of the biases vary between -2 K and 1 K . Biases observed in the Northern Hemisphere are in general comparable to biases observed in the Southern Hemisphere. Spectra obtained in the tropics are more articulate and the biases observed in this region are larger than the biases observed in the other geographical regions. In addition, the differences between the spectra obtained in the tropics are larger than the differences between the spectra obtained elsewhere. In all geographical regions, the larger biases are seen in correspondence of channels located in the spectral region characterized by the presence of the strong ν_4 -band of methane at 1310 cm^{-1} where negative values are in general observed. The larger biases in this region can be partly explained by the fact that

The accuracy of the RTTOV fast radiative transfer model

M. Matricardi

[Title Page](#)

[Abstract](#)

[Introduction](#)

[Conclusions](#)

[References](#)

[Tables](#)

[Figures](#)

◀

▶

◀

▶

[Back](#)

[Close](#)

[Full Screen / Esc](#)

[Printer-friendly Version](#)

[Interactive Discussion](#)



methane amounts are fixed to climatological values.

LBLRTM and kCARTA spectra exhibit very similar features in the left side and central part of the water vapour ν_2 band from 1400 up to 1700 cm^{-1} . In this spectral region the GENLN2 spectrum is more irregular and probably reflects differences in the spectroscopy. This is all the more evident around 1600 cm^{-1} where GENLN2 shows significantly larger biases. We interpret this result in terms of the GENLN2 water vapour continuum model. In fact, in the spectral region around 1600 cm^{-1} the GENLN2 continuum model uses significantly smaller values of the spectral density function (see Fig. 2). To the right side of the band, the structure of the spectra is more irregular. The GENLN spectrum follows more closely the LBLRTM spectrum and in the case of kCARTA we can observe a consistent number of spikes that are not present in the spectra obtained using the other LBL models. This is very apparent around 1740 and 1800 cm^{-1} . In general, it would appear that LBLRTM tends to fit better the observations although it is difficult to give a conclusive answer since the results can be affected by uncertainties in the water vapour profiles above all in presence of the high water vapour loadings characteristic of tropical conditions. However, we should also note that in the tropics and in the Southern Hemisphere the LBLRTM spectra between 1980 and 2000 cm^{-1} exhibit larger biases than the GENLN2 and kCARTA spectra.

Since GENLN2 and kCARTA use the same molecular database it is difficult to explain the origin of the large spikes in the kCARTA spectra since these cannot be attributed to the continuum model as shown in the upper panel of Fig. 11. In this panel, we have plotted the difference between the standard kCARTA spectrum and the kCARTA spectrum computed in the tropical region using the LBLRTM continuum (kCARTA_LBL). The spectrum in the upper panel of Fig. 11 shows that in IASI band 2, differences between the kCARTA and LBLRTM continuum can only have a significant impact in the regions at the edges of the band. Hence, the vast majority of the spikes seen in kCARTA cannot be attributed to the continuum model. The same conclusion also applies to the spectra obtained in the other geographical regions although the results are not shown here. It could be argued that the kCARTA spikes could be a feature

The accuracy of the RTTOV fast radiative transfer model

M. Matricardi

[Title Page](#)

[Abstract](#)

[Introduction](#)

[Conclusions](#)

[References](#)

[Tables](#)

[Figures](#)

◀

▶

◀

▶

[Back](#)

[Close](#)

[Full Screen / Esc](#)

[Printer-friendly Version](#)

[Interactive Discussion](#)



of the fast transmittance model used in RTTOV. However, in IASI band 1 and IASI band 2 the predictors used to compute the kCARTA coefficients are the same as those used for the LBLRTM and GENLN2 coefficients. Although the computation of the water vapour coefficients involve the weighting of the input data prior to the regression, to our knowledge the details of the procedure used to perform this operation for the kCARTA coefficients does not differ from the procedure adopted for the GENLN2 and LBLRTM coefficients.

Finally, in the lower panel of Fig. 11 we have superimposed the tropical spectra that show the difference between the kCARTA mean spectrum and the LBLRTM mean spectrum and the difference between the kCARTA_LBL mean spectrum and the LBLRTM mean spectrum. The spectra in the lower panel of Fig. 11 show that differences between kCARTA and LBLRTM in the region between 1970 and 1990 cm⁻¹ and between 1200 and 1280 cm⁻¹ are almost entirely attributable to the continuum model. The same can be said for the spectra in the Southern Hemisphere although the results are not shown here.

5.3 IASI band 3 (2000 to 2760 cm⁻¹)

Results for IASI band 3 are shown in Figs. 12, 13, and 14 for the Northern Hemisphere, tropics and Southern Hemisphere, respectively. The larger biases between 2080 and 2200 cm⁻¹ in the Southern Hemisphere and in the tropics reflect latitudinal gradients of CO amounts not accounted for in the RT computations. In the same spectral region biases in the Northern Hemisphere vary between -0.4 K and 0.4 K reflecting smaller CO latitudinal gradients in this geographical region. Very noticeable are the large spikes in the kCARTA spectra between 2000 and 2150 cm⁻¹.

5.3.1 Results in the temperature sounding band

The biases observed in the ν_3 -CO₂ band are larger than the biases observed in the ν_2 -band. Among the factors that can contribute to this result we can include the ac-

The accuracy of the RTTOV fast radiative transfer model

M. Matricardi

[Title Page](#)

[Abstract](#)

[Introduction](#)

[Conclusions](#)

[References](#)

[Tables](#)

[Figures](#)

◀

▶

◀

▶

[Back](#)

[Close](#)

[Full Screen / Esc](#)

[Printer-friendly Version](#)

[Interactive Discussion](#)



curacy of the spectroscopic parameters and biases in the ECMWF stratospheric and mesospheric temperature profiles. In particular, temperature biases could play an important role in a spectral region that sees the presence of a large number of channels characterized by very high-peaking weighting functions with tails that can extend well into 0.2 hPa. It should also be noted that because of the symmetry of the states involved in the molecular transitions, P/R-branch line mixing is expected to be twice as strong than in the ν_2 -band.

Between 2200 and 2380 cm^{-1} , biases in the Northern and Southern Hemisphere assume negative values that vary between -1.8 K and -0.4 K . LBLRTM and GENLN
10 exhibit larger biases around 2260 cm^{-1} whereas kCARTA exhibits larger biases around 2280 cm^{-1} . Biases between 2320 and 2380 cm^{-1} are very similar for all models. In the tropical region we observe the same general pattern. However, when compared to results obtained in the other geographical regions, biases between 2320 and 2380 cm^{-1} are now smaller whereas biases around 2280 cm^{-1} are now much larger with GENLN2
15 attaining values as large as -3 K . The similarity between the GENLN2 and LBLRTM spectra is noticeable and we tend to attribute this feature to the line mixing model used in the LBL codes.

As shown in our plots, GENLN2 spectra in the region between 2380 and 2400 cm^{-1} (i.e. the far wing of the R-branch of the ν_3 band) exhibit biases that are typically larger
20 than the biases observed in the equivalent kCARTA and LBLRTM spectra. Given the importance of P/R-branch line mixing in this region, we tend interpret this result as a consequence of errors in the GENLN2 Cousin CO_2 line shape. If the behaviour of GENLN2 is justified on the grounds of inaccurate line shape, the LBLRTM spectra show that there are still issues with the modelling of CO_2 line shape in the $\text{CO}_2 \nu_3$ -bandhead.
25 This is also true, albeit to a much lesser extent, for kCARTA. In particular, between 2380 and 2400 cm^{-1} the LBLRTM spectra show large oscillations whose amplitude can reach almost 3 K in the Northern Hemisphere. It is possible that this result could be associated to biases in the ECMWF temperature profiles but we would like to bring forward the hypothesis that this behaviour might in fact be related to the treatment of the

The accuracy of the RTTOV fast radiative transfer model

M. Matricardi

[Title Page](#)

[Abstract](#)

[Introduction](#)

[Conclusions](#)

[References](#)

[Tables](#)

[Figures](#)

◀

▶

◀

▶

[Back](#)

[Close](#)

[Full Screen / Esc](#)

[Printer-friendly Version](#)

[Interactive Discussion](#)



CO₂ continuum in LBLRTM. Our spectra could indicate that the scaling factor of 0.75 applied to the CO₂ continuum might not be universally valid. This hypothesis seems to be corroborated by the results obtained by Masiello et al. (2009) using aircraft data. They show that changing the scaling factor to the value used in a previous release of
5 LBLRTM can improve the accuracy of the spectra.

5.3.2 Results in the window region

Biases in the 2500 cm⁻¹ window region tend to be influenced by the same factors discussed in Sect. 5.1.3. It should be noted that the water vapour continuum in band 3 is known to a lesser accuracy than in band 1. As in band 1, spectra in the Northern
10 and Southern Hemispheres are closer than spectra in the tropics. However, opposite to what observed in band 1, biases in the Southern Hemisphere tend to be larger than biases in the Northern Hemisphere. Biases are generally negative but a small number of positive values are also observed. In terms of absolute values, biases vary between –0.4 and 0.8 K.

Differences between the spectra largely reflect differences between the continua
15 models. The top panel in Fig. 15 shows the difference between kCARTA and kCARTA_LBL in the tropical region and illustrates how the change of the continuum model has an impact between 2380 and 2660 cm⁻¹. The bottom panel shows that the use of the same continuum model has reduced to naught differences between kCARTA
20 and LBLRTM in the 2440 to 2624 cm⁻¹ spectral region. Hence, in this spectral region differences between kCARTA and LBLRTM can be attributed solely to the continuum; it would also appear that the kCARTA spectra are in better agreement with observation suggesting that the modifications made to the continuum model have improved the accuracy of RT computations. It should also be noted that, as shown in Fig. 15, between
25 2400 and 2440 cm⁻¹ most of the differences between the LBLRTM and kCARTA spectra cannot be attributed to the continuum. In this spectral interval, the broad features of the LBLRTM spectra are more similar to the features of the GENLN2 spectra than to the features of the kCARTA spectra. A possible explanation of this behaviour could

| | |
|--|------------------------------|
| Title Page | |
| Abstract | Introduction |
| Conclusions | References |
| Tables | Figures |
| ◀ | ▶ |
| ◀ | ▶ |
| Back | Close |
| Full Screen / Esc | |
| Printer-friendly Version | |
| Interactive Discussion | |



lie in the implementation of the CO₂ continuum. The implementation of the Nitrogen continuum absorption might also play a role although it is an unlikely factor given the fact that kCARTA and LBLRTM use the same model.

Beyond 2624 cm⁻¹, differences between the spectra are attributable to the water vapour spectroscopy. This is clearly demonstrated by the fact the kCARTA spectra are in better agreement with the GENLN2 spectra (the two models use the same molecular database). In this region dominated by line absorption, results tend to suggest that the spectroscopic parameters used in LBLRTM fit marginally better the observations.

6 Conclusions

- Four monitoring experiments have been carried out to compare IASI observed radiances to radiances simulated by the RTTOV fast radiative transfer model using regression coefficients based on the GENLN2, kCARTA and LBLRTM LBL models using different molecular databases. Results obtained from IASI data between the 1 April 2008 and the 15 April 2008 using clear channels (i.e. channels not affected by clouds) over the sea show that in the northern and Southern Hemisphere biases in IASI band 1 and 2 are typically within ±1 K. In the tropics, biases in the water vapour ν2-band do increase but for most of the channels the peak-to-peak value is still within within ±1 K. The larger biases observed in the water vapour band tend to reflect errors in line parameters generated by spectroscopic errors and by the inaccurate specification of the water vapour profiles. The use of the MT_CKD continuum model results in a reduction up to 1 K of the biases in the region around 1600 cm⁻¹. The large biases observed in the ozone band in the Northern Hemisphere probably reflect a poorer performance of the ozone assimilation system in this geographical region. A more accurate description of the CO₂ line shape has a significant impact on the simulated radiances in the CO₂ ν2-band resulting in a reduction of the biases up to 1 K. In the same band, line mixing coefficients based on a first order perturbation theory appear not to be adequate to model the absorption in the Q-branch at 667 cm⁻¹. In the important temperature

The accuracy of the RTTOV fast radiative transfer model

M. Matricardi

[Title Page](#)

[Abstract](#)

[Introduction](#)

[Conclusions](#)

[References](#)

[Tables](#)

[Figures](#)

◀

▶

◀

▶

[Back](#)

[Close](#)

[Full Screen / Esc](#)

[Printer-friendly Version](#)

[Interactive Discussion](#)



- sounding CO₂ ν_3 -band we obtained biases significantly larger than biases observed in the ν_2 -band and we tend to attribute this result to spectroscopic errors and to biases in the ECMWF temperature profiles. Since the ν_3 -band contains a consistent number of very good temperature sounding channels placed in spectral regions where the interference of different absorbing species is minimal, it is important that updated CO₂ ν_3 -band line parameters be made available to help reducing errors in this band. The kCARTA and LBLRTM improvements in the CO₂ line shape result in smaller biases in the CO₂ ν_3 -band head. However, the LBLRTM spectra display large oscillations not seen in the kCARTA spectra. We have tentatively suggested that this behaviour might be due to the value used for the scaling factor utilized in the LBLRTM CO₂ continuum model. Finally, we want to conclude by noting that we are aware of the limitations inherent in the study of RT and spectroscopic errors using an NWP environment. We have stressed, for instance, that systematic profile errors can affect the results. However, an NWP system offers the unique possibility of using a very robust statistical sample made of a large number of data obtained in very diverse conditions. In many instances, results obtained in this study are consistent with results obtained by using aircraft data in very controlled atmospheric situations albeit their interpretation may differ. This encourages us in continuing pursuing this effort above all in the light of the continuous improvements made in NWP.
- Acknowledgements. IASI has been developed and built under the responsibility of the Centre National d'Etudes Spatiales (CNES, France). It is flown onboard the Metop satellites as part of the EUMETSAT Polar System. The IASI L1 data are received through the EUMETCast near real time data distribution service. We want to thank P. Brunel (Météo France) for having made available the kCARTA coefficients, C. Clerbaux (Service d'Aéronomie) for having made available concentrations for minor gas species, T. McNally (ECMWF) for the very helpful collaboration received during the set up of the monitoring experiments and A. Collard (ECMWF) and N. Bormann (ECMWF) for the implementation of IASI and RTTOV-9 in the ECMWF data assimilation system.

The accuracy of the RTTOV fast radiative transfer model

M. Matricardi

[Title Page](#)

[Abstract](#)

[Introduction](#)

[Conclusions](#)

[References](#)

[Tables](#)

[Figures](#)

◀

▶

◀

▶

[Back](#)

[Close](#)

[Full Screen / Esc](#)

[Printer-friendly Version](#)

[Interactive Discussion](#)



- 5 Aumann, H. H., Chahine, M. T., Gautier, C., Goldberg, M. D., Kalnay, E., McMillin, L. M., Revercomb, H., Rosenkranz, P. W., Smith, W. L., Staelin, D. H., Strow, L. L., and Susskind, J.: AIRS/AMSU/HSB on the Aqua mission: design, science objectives, data products, and processing systems, *Geoscience and Remote Sensing, IEEE Transactions on* Volume 41(2), 253–264, 2003.
- 10 Brunel, P. and Turner, S.: On the use of Planck-weighted transmittances in RTTOV, *Proceedings of the 13th International TOVS study conference, Ste Adele, Canada,* http://cimss.ssec.wisc.edu/itwg/itsc/itsc13/thursday/brunel_poster.pdf, 2003.
- 15 Chalon, G., Cayla, F., and Diebel, D.: IASI: An Advanced Sounder for Operational Meteorology, *Proceedings of the 5th Congress of IAF, Tolouse, France*, 1.5, 2001.
- Chevallier, F.: Sampled database of 60-level atmospheric profiles from the ECMWF analyses, ECMWF, NWP SAF, Report no. NWPSAF-EC-TR-001, 2000.
- 20 Clough, S. A., Kneizys, F. X., and Davis, R. W.: Line shape and the water vapour continuum, *Atmos. Res.*, 23, 229–241, 1989.
- Clough, S. A., Iacono, M. J., and Moncet J.-L.: Line by line calculation of atmospheric fluxes and cooling rates: application to water vapor, *J. Geophys. Res.*, 98, 15761–15785, 1992.
- 25 Collard, A. D. and McNally, A. P.: Assimilation of IASI radiances at ECMWF, *Q. J. Roy. Meteor. Soc.*, in review, 2008.
- 30 Cousin, C., Le Doucen, R., Boulet, C., and Henry, H.: Temperature dependence of the absorption in the region beyond the $4.3\text{ }\mu\text{m}$ band head of CO₂, Part 2: N₂ and O₂ broadening, *Appl. Optics*, 24, 3899–3907, 1985.
- De Souza-Machado, S., Strow, L. L., Tobin, D., Motteler, H., and Hannon, S. E.: Improved atmospheric radiance calculations using CO₂ p/r-branch line mixing, in: *Proc. Euro. Symp. Aerospace Remote Sensing Europto Series*, 188–195, 1999.
- 25 De Souza-Machado, S., Strow, L. L., Motteler, H., and Hannon, S. E.: kCARTA: an atmospheric radiative transfer algorithm using compressed lookup tables, Univ. Maryland Baltimore County, Dept. Physics, Tech. Report, available at <http://asl.umbc.edu/pub/rta/kcarta>, 2002.
- 30 Edwards, D. P.: GENLN2, A general Line-by-Line Atmospheric Transmittance and Radiance Model, NCAR Technical note NCAR/TN-367+STR, National Center for Atmospheric Research, Boulder, Co, 1992.

The accuracy of the RTTOV fast radiative transfer model

M. Matricardi

[Title Page](#)

[Abstract](#)

[Introduction](#)

[Conclusions](#)

[References](#)

[Tables](#)

[Figures](#)

◀

▶

◀

▶

[Back](#)

[Close](#)

[Full Screen / Esc](#)

[Printer-friendly Version](#)

[Interactive Discussion](#)



- Eyre, J. R. and Woolf, H. M.: Transmittance of atmospheric gases in the microwave region: a fast model, *Appl. Optics*, 27, 3244–3249, 1988.
- Hauglustaine, D. A., Brasseur, G. P., Walters, S., Rasch, P. J., Müller, J.-F., Emmons, L. K., and Carroll, M. A.: MOZART, a global chemical transport model for ozone and related chemical tracers, 2, Model results and evaluation, *J. Geophys. Res.*, 103, 28, 291–28, 335, 1998.
- Jacquinet-Husson, N., Scott, N. A., Chedin, A., Garceran, K., Armante, R., Chursin, A. A., Barbe, A., Birk, M., Brown, L. R., Camy-Peyret, C., Claveau, C., Clerbaux, C., Coheur, P. F., Dana, V., Daumont, L., Debacker-Barily, M. R., Flaud, J. M., Goldman, A., Hamdouni, A., Hess, M., Jacquemart, D., Kopke, P., Mandin, J. Y., Massie, S., Mikhailenko, S., Nemtchinov, V., Nikitin, A., Newnham, D., Perrin, A., Perevalov, V. I., Regalia-Jarlot, L., Rublev, A., Schreier, F., Schult, I., Smith, K. M., Tashkun, S. A., Teffo, J. L., Toth, R. A., Tyuterev, Vl. G., Vander Auwera, J., Varanasi, J. P., and Wagner, G.: The 2003 edition of the GEISA/IASI spectroscopic database, *J. Quant. Spectrosc. Radiat. Transfer*, 95, 429–467, 2005.
- Kara, A. B. and Barron, C. N.: Fine-resolution satellite-based daily sea surface temperatures over the global ocean, *J. Geophys. Res.*, 112, C05041, doi:10.1029/2006JC004021, 2007.
- Lafferty, W. J., Solodov, A. M., Weber, A., Olson, W. B. and Hartman, J-M.: Infrared collision-induced absorption by N₂ near 4.3 μm for atmospheric applications: measurements and empirical modelling, *Appl. Optics*, 35, 5911–5917, 1996.
- Ma, Q., Tipping, R. H., and Leforestier, C.: Temperature dependences of mechanisms responsible for the water-vapor continuum absorption: 1. Far wings of allowed lines, *J. Chem. Phys.*, 128, 124313, doi:10.1063/1.2839604, 2008.
- Masiello, G., Serio, C., Carissimo, A., Grieco, G., and Matricardi, M.: Application of ϕ -IASI to IASI: retrieval products evaluation and radiative transfer consistency, *Atmos. Chem. Phys.*, in review, 2009.
- Matricardi, M. and Saunders, R.: Fast Radiative Transfer Model for Simulation of Infrared Atmospheric Sounding Interferometer Radiances, *Appl. Optics*, 38, 5679–5691, 1999.
- Matricardi, M.: RTIASI-4, a new version of the ECMWF fast radiative transfer model for the infrared atmospheric sounding interferometer, ECMWF Research, Dept. Tech. Memo., 345, <http://www.ecmwf.int/publications>, 2003.
- Matricardi, M., Chevallier, F., Kelly, G., and Thepaut, J.-N.: An improved general fast radiative transfer model for the assimilation of radiance observations, *Q. J. Roy. Meteorol. Soc.*, 130, 153–173, 2004.
- Matricardi, M.: An inter-comparison of line-by-line radiative transfer models, ECMWF Research

The accuracy of the RTTOV fast radiative transfer model

M. Matricardi

[Title Page](#)

[Abstract](#)

[Introduction](#)

[Conclusions](#)

[References](#)

[Tables](#)

[Figures](#)

◀

▶

[Back](#)

[Close](#)

[Full Screen / Esc](#)

[Printer-friendly Version](#)

[Interactive Discussion](#)



- Dept. Tech. Memo., 525, <http://www.ecmwf.int/publications>, 2007.
- Matricardi, M.: The generation of RTTOV regression coefficients for IASI and AIRS using a new profile training set and a new line-by-line database, ECMWF Research Dept. Tech. Memo., 564, <http://www.ecmwf.int/publications>, 2008.
- 5 McNally, A. P. and Watts, P. D.: A cloud detection algorithm for high-spectral-resolution infrared sounders, *Q. J. Roy Meteorol. Soc.*, 129, 3411–3423, 2003.
- McNally, A. P., Watts, P. D., Smith, J. A., Engelen, R., Kelly, G. A., Thepaut, J. N., and Matricardi, M.: The assimilation of AIRS radiance data at ECMWF, *Q. J. Roy. Meteorol. Soc.*, 132, 935–957, 2006.
- 10 Menoux, V., Le Doucen, R., Boulet, C., Roblin, A., and Bouchardy, A. M: Collision induced absorption in the fundamental Band of N₂, *Appl. Optics*, 32, 263–268, 1993.
- Niro, F., Jucks, K., and Hartmann, J.-M.: Spectra calculations in central and wing regions of CO₂ IR bands, IV: software and database for the computation of atmospheric spectra, *Journal of Quantitative Spectroscopy and Radiative Transfer*, 95(4), 469–481, 2005.
- 15 Rabier, F., Thepaut, J.-N., and Courtier, P.: Extended assimilation and forecast experiments with a four dimensional variational assimilation scheme, *Q. J. Roy. Meteorol. Soc.*, 132, 935–957, 1998.
- Rinsland, C. P., Zander, J. S., Namkung, J. S., Farmer, C. B., and Norton, R. H.: Stratospheric infrared continuum absorption observed by the ATMOS instrument, *J. Geophys. Res.*, 94, 20 16303–16322, 1989.
- Rizzi, R., Matricardi, M., and Miskolczi, F.: Simulation of Uplooking and Downlooking High-Resolution Radiance Spectra With Two Different Radiative Transfer models, *Appl. Optics*, 41, 940–956, 2002.
- 25 Rothman, L. S., Barbe, A., Chris Benner, D., Brown, L. R., Camy-Peyret, C., Carleer, M. R., Chance, K., Clerbaux, C., Dana, V., Devi, V. M., Fayt, A., Flaud, J.-M., Gamache, R. R., Goldman, A., Jacquemart, D., Jucks, K. W., Lafferty, W. J., Mandin, J.-Y., Massie, S. T., Nemtchinov, V., Newnham, D. A., Perrin, A., Rinsland, C. P., Schroeder, J., Smith, K. M., Smith, M. A. H., Tang, K., Toth, R. A., Vander Auwera , J., Varanasi, P., Yoshino, K.: The HITRAN molecular spectroscopic database: edition of 2000 including updates through 2001, *J. Quant. Spectrosc. Radiat. Transfer*, 82, 5–44, 2003.
- 30 Rothman, L. S., Jacquemart, D., Barbe, A., Chris Benner, D., Birk, M., Brown, L. R., Carleer, M. R., Chackerian Jr., C., Chance, C. K., Coudert, L. H., Dana, V., Devi, V. M., Flaud, J. M., Gamache, R. R., Goldman, A., Hartmann, J. M., Jucks, K. W., Maki, A. G., Mandin, J. Y.,

The accuracy of the RTTOV fast radiative transfer model

M. Matricardi

[Title Page](#)

[Abstract](#)

[Introduction](#)

[Conclusions](#)

[References](#)

[Tables](#)

[Figures](#)



[Back](#)

[Close](#)

[Full Screen / Esc](#)

[Printer-friendly Version](#)

[Interactive Discussion](#)



- Massie, S. T., Orphal, J., Perrin, A., Rinsland, C. P., Smith, M. A. H., Tennyson, J., Tolchenov, R. N., Toth, R. A., Vander Auwera, J., Varanasi, P., Wagner, G.: The HITRAN 2004 molecular spectroscopic database, *J. Quant. Spectrosc. Radiat. Transfer*, 96, 139–204, 2005.
- Saunders, R., Matricardi, M., and Brunel, P.: An improved fast radiative transfer model for atmospheric simulation of satellite radiance observations, *Quart. J. Roy. Meteor. Soc.*, 144, 1547–1558, 1999.
- Saunders, R., Matricardi, M., and Geer, A.: Rttov9.1 users guide, NWP SAF report, Met. Office, 57 pp., 2008.
- Sherlock, V.: ISEM-6: Infrared Surface Emissivity Model for RTTOV-6, NWP SAF report, <http://www.metoffice.gov.uk/research/interproj/nwpasaf/rtm/papers/isem6.pdf>, 1999.
- Smith, W. L., Woolf, H. M., Hayden, C. M., Wark, D. Q., and McMillin, L. M.: The TIROS-N Operational Vertical Sounder, *Bull. Am. Meteorol. Soc.*, 60, 1177–1187, 1979.
- Strow, L. L. and Reuter, D.: Effect of line mixing on atmospheric brightness temperatures near 15 μm , *Appl. Optics*, 27, 872–878, 1988.
- Strow, L. L., Tobin, D. C., and Hannon, S. E.: A compilation of First-Order Line-Mixing coefficients for CO₂ Q-branches, *J. Quant. Spectrosc. Radiat. Transfer*, 52, 281–294, 1994.
- Strow, L. L., Motteler, H. E., Benson, R. G., Hannon, S. E., and De Souza-Machado, S.: Fast computation of monochromatic infrared atmospheric transmittances using compressed lookup tables, *J. Quant. Spectrosc. Radiat. Transfer*, 59, 481–493, 1998.
- Strow, L. L., Hannon, S. E., De Souza-Machado, S., Motteler, S. H., and Tobin, D.: An Overview of the AIRS Radiative Transfer Model, *IEEE Transactions on GeoSciences and Remote Sensing*, 41, 274 pp., 2003.
- Tibault, F., Menoux, V., Le Doucen, R., Rosenman, L., Hartman, J.-M., and Boulet, C.: Infrared collision induced absorption by O₂ near 6.4 microns for atmospheric applications: measurements and empirical modeling, *Appl. Optics*, 36, 563–567, 1997.
- Timofeyev, Y. M. and Tonkov, M. V.: Effect of the induced Oxygen absorption band on the transformation of radiation in the 6 μm region of the Earth's atmosphere, *Atmos. Ocean Phys.*, 14, 437–441, 1978.
- Tjemkes, S. A., Patterson, T., Rizzi, R., Shephard, M. W., Clough, S. A., Matricardi, M., Haigh, J. D., Höpfner, M., Payan, S., Trotsenko, A., Scott, N., Rayer, P., Taylor, J. P., Clerbaux, C., Strow, L. L., DeSouza-Machado, S., Tobin, D., and Knuteson, R.: The ISSWG line-by-line inter-comparison experiment, *J. Quant. Spectrosc. Radiat. Transfer*, 77, 433–453, 2003.
- Tobin, D. C.: Infrared spectral lineshapes of water vapour and carbon dioxide, Ph.D. dissertation, 30

The accuracy of the RTTOV fast radiative transfer model

M. Matricardi

[Title Page](#)

[Abstract](#)

[Introduction](#)

[Conclusions](#)

[References](#)

[Tables](#)

[Figures](#)

◀

▶

◀

▶

[Back](#)

[Close](#)

[Full Screen / Esc](#)

[Printer-friendly Version](#)

[Interactive Discussion](#)



tion, Univ. Maryland Baltimore County, Baltimore, MD, 1996.

Tobin, D. C., Best, F. A., Brown, P. D., Clough, S. A., Dedecker, R. G., Ellingson, R. G., Garcia, R. K., Howell, H. B., Knuteson, R. O., Mlawer, E. J., Revercomb, H. E., Short, J. F., van Delst, P. F. W., and Walden, V. P.: Downwelling spectral radiance observations at the SHEBA ice station: Water vapor continuum measurements from 17 to 26 μm , *J. Geophys. Res.*, 4(D2), 2081–2092, 1999.

ACPD

9, 9491–9535, 2009

The accuracy of the RTTOV fast radiative transfer model

M. Matricardi

[Title Page](#)

[Abstract](#)

[Introduction](#)

[Conclusions](#)

[References](#)

[Tables](#)

[Figures](#)

◀

▶

◀

▶

[Back](#)

[Close](#)

[Full Screen / Esc](#)

[Printer-friendly Version](#)

[Interactive Discussion](#)



The accuracy of the RTTOV fast radiative transfer model

M. Matricardi

Table 1. The regression coefficients used for the RTTOV simulations.

| Coefficients | Continuum | CO ₂ line mixing | Molecular Database |
|--|-------------------|---|---|
| LBL model: kCARTA Number of levels: 101 Profile training set: ECMWF_52_P | MTK_CKD.v1.1_UMBC | P/Q/R branch (ν_2 and ν_3 band) | HITRAN_2000 |
| LBL model: GENLN2 Number of levels: 101 Profile training set: ECMWF_43_P | CKD_v2.4 | Q branch (ν_2 and ν_3 band) | HITRAN_2000 |
| LBL model: LBLRTM Number of levels: 101 Profile training set: ECMWF_83_P | MTK_CKD_v2.2 | P/Q/R branch (ν_2 and ν_3 band) | HITRAN_2000 HITRAN_2004/2006 GEISA_2003 |

[Title Page](#)

[Abstract](#)

[Introduction](#)

[Conclusions](#)

[References](#)

[Tables](#)

[Figures](#)

◀

▶

◀

▶

[Back](#)

[Close](#)

[Full Screen / Esc](#)

[Printer-friendly Version](#)

[Interactive Discussion](#)



Self broadening

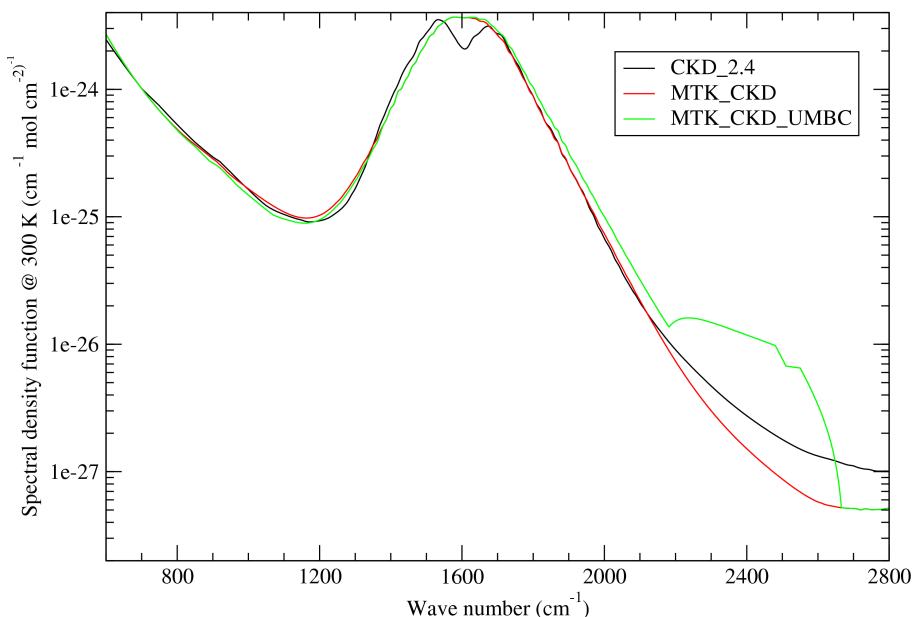


Fig. 1. Spectral density function for the water vapour self broadening coefficients at 300 K and 1013 hPa.

The accuracy of the RTTOV fast radiative transfer model

M. Matricardi

[Title Page](#)[Abstract](#)[Introduction](#)[Conclusions](#)[References](#)[Tables](#)[Figures](#)[◀](#)[▶](#)[Back](#)[Close](#)[Full Screen / Esc](#)[Printer-friendly Version](#)[Interactive Discussion](#)

Foreign broadening

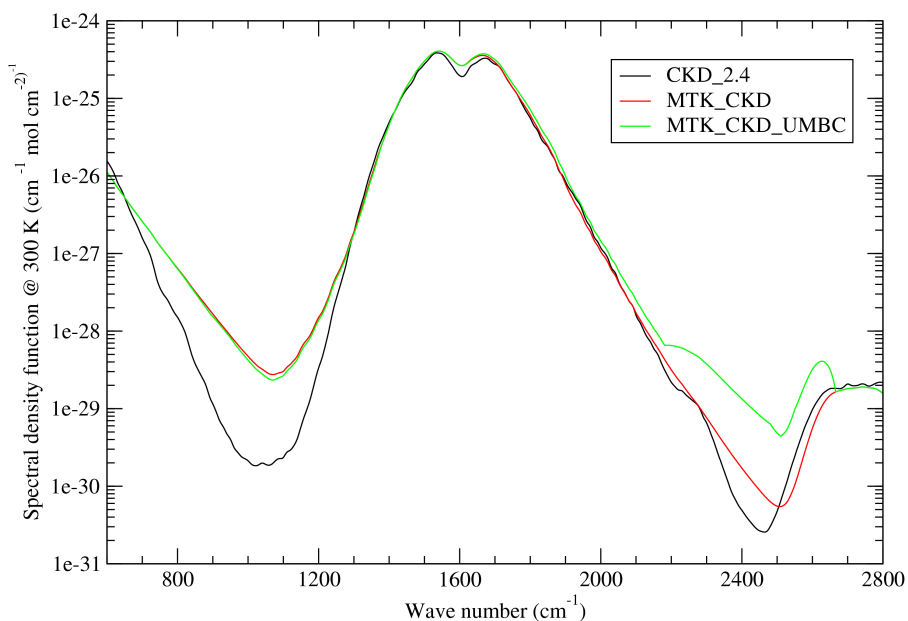


Fig. 2. Spectral density function for the water vapour foreign broadening coefficients at 300 K and 1013 hPa.

The accuracy of the RTTOV fast radiative transfer model

M. Matricardi

[Title Page](#)

[Abstract](#)

[Introduction](#)

[Conclusions](#)

[References](#)

[Tables](#)

[Figures](#)

[◀](#)

[▶](#)

[◀](#)

[▶](#)

[Back](#)

[Close](#)

[Full Screen / Esc](#)

[Printer-friendly Version](#)

[Interactive Discussion](#)



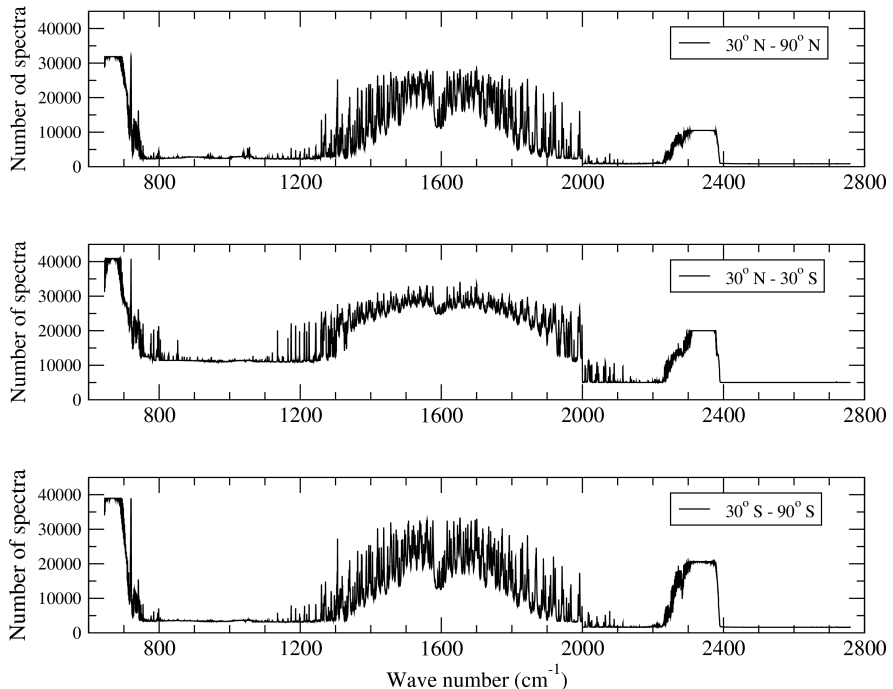


Fig. 3. The number of spectra sampled as clear for each IASI channel for three different latitude bands.

The accuracy of the RTTOV fast radiative transfer model

M. Matricardi

[Title Page](#)

[Abstract](#)

[Introduction](#)

[Conclusions](#)

[References](#)

[Tables](#)

[Figures](#)

◀

▶

[Back](#)

[Close](#)

[Full Screen / Esc](#)

[Printer-friendly Version](#)

[Interactive Discussion](#)



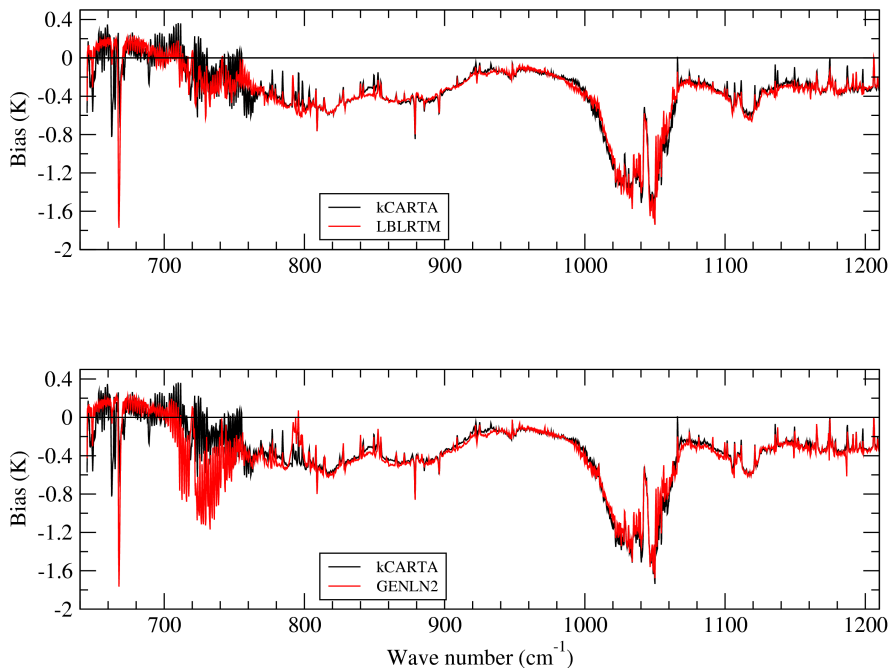


Fig. 4. The mean value of the difference between observed and computed brightness temperatures in the Northern Hemisphere for IASI band 1.

The accuracy of the RTTOV fast radiative transfer model

M. Matricardi

[Title Page](#)

[Abstract](#)

[Introduction](#)

[Conclusions](#)

[References](#)

[Tables](#)

[Figures](#)

◀

▶

[Back](#)

[Close](#)

[Full Screen / Esc](#)

[Printer-friendly Version](#)

[Interactive Discussion](#)



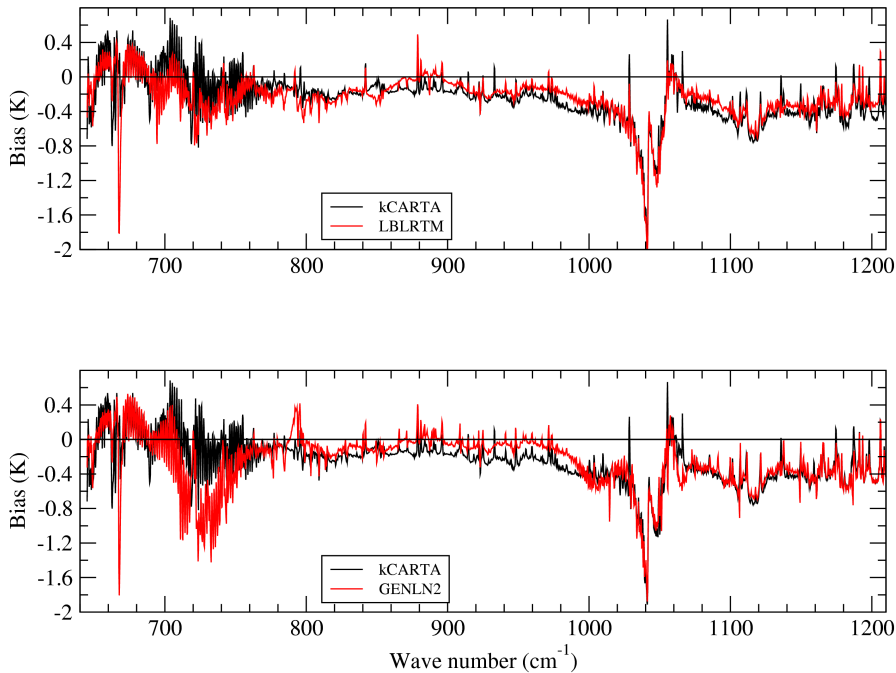


Fig. 5. The mean value of the difference between observed and computed brightness temperatures in the tropical region for IASI band 1.

The accuracy of the RTTOV fast radiative transfer model

M. Matricardi

[Title Page](#)

[Abstract](#)

[Introduction](#)

[Conclusions](#)

[References](#)

[Tables](#)

[Figures](#)

◀

▶

[Back](#)

[Close](#)

[Full Screen / Esc](#)

[Printer-friendly Version](#)

[Interactive Discussion](#)



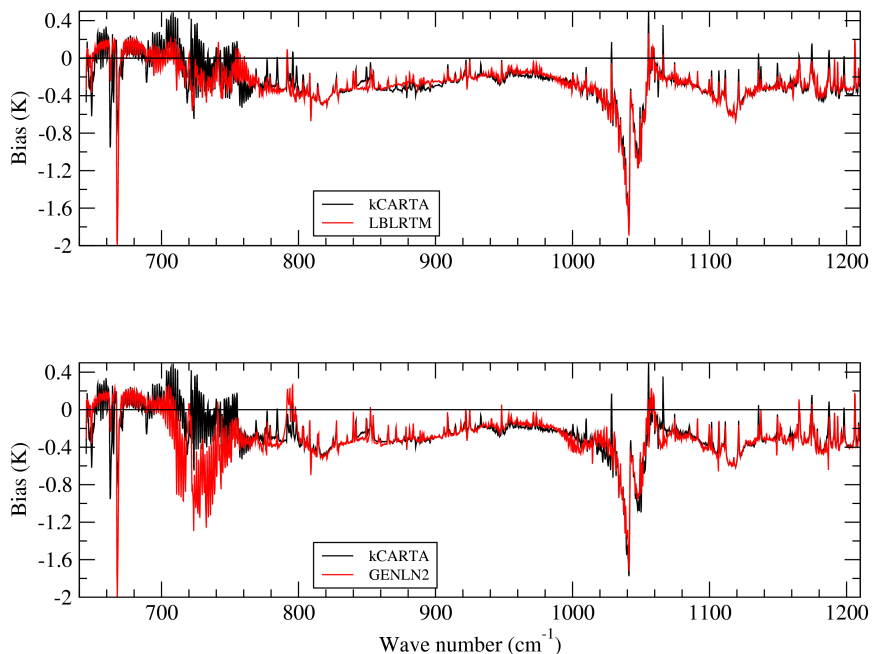


Fig. 6. The mean value of the difference between observed and computed brightness temperatures in the Southern Hemisphere for IASI band 1.

The accuracy of the RTTOV fast radiative transfer model

M. Matricardi

[Title Page](#)

[Abstract](#)

[Introduction](#)

[Conclusions](#)

[References](#)

[Tables](#)

[Figures](#)

[◀](#)

[▶](#)

[Back](#)

[Close](#)

[Full Screen / Esc](#)

[Printer-friendly Version](#)

[Interactive Discussion](#)



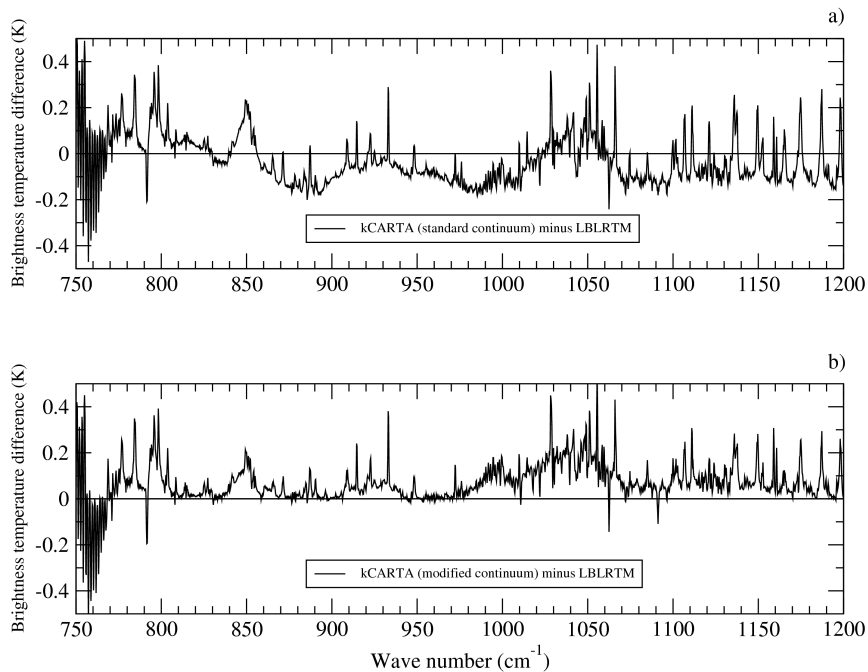


Fig. 7. The difference between (a) kCARTA and LBLRTM in the tropical region; (b) kCARTA_LBL and LBLRTM in the tropical region.

The accuracy of the RTTOV fast radiative transfer model

M. Matricardi

[Title Page](#)

[Abstract](#)

[Introduction](#)

[Conclusions](#)

[References](#)

[Tables](#)

[Figures](#)

◀

▶

[Back](#)

[Close](#)

[Full Screen / Esc](#)

[Printer-friendly Version](#)

[Interactive Discussion](#)



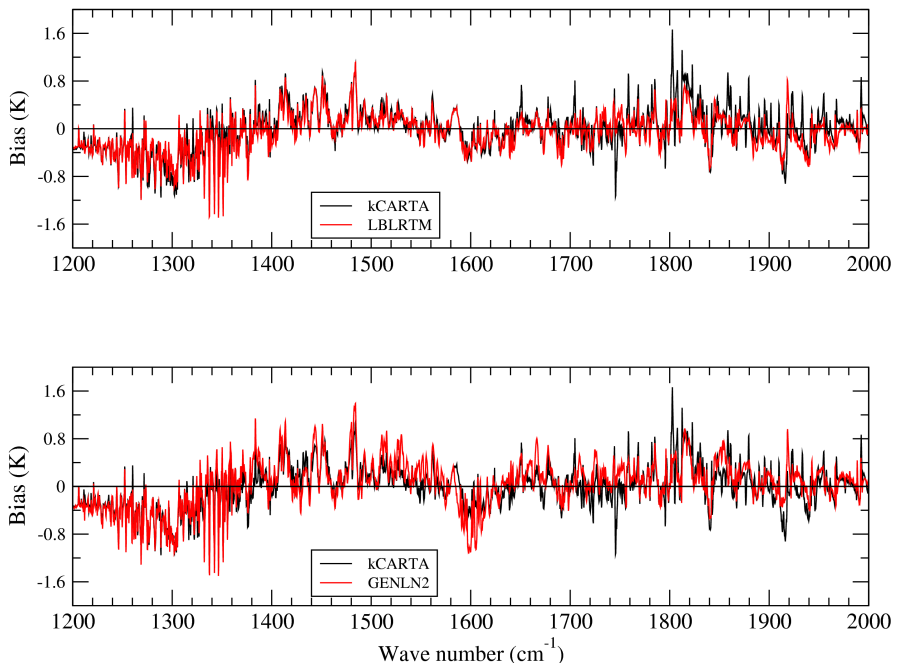


Fig. 8. The mean value of the difference between observed and computed brightness temperatures in the Northern Hemisphere for IASI band 2.

The accuracy of the RTTOV fast radiative transfer model

M. Matricardi

[Title Page](#)

[Abstract](#)

[Introduction](#)

[Conclusions](#)

[References](#)

[Tables](#)

[Figures](#)

◀

▶

◀

▶

[Back](#)

[Close](#)

[Full Screen / Esc](#)

[Printer-friendly Version](#)

[Interactive Discussion](#)



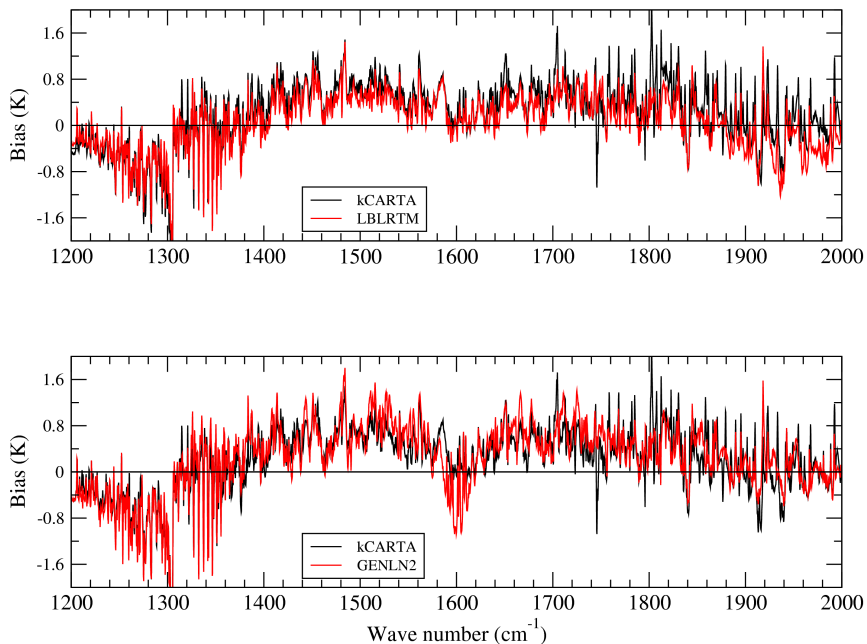


Fig. 9. The mean value of the difference between observed and computed brightness temperatures in the tropical region for IASI band 2.

The accuracy of the RTTOV fast radiative transfer model

M. Matricardi

[Title Page](#)

[Abstract](#)

[Introduction](#)

[Conclusions](#)

[References](#)

[Tables](#)

[Figures](#)

◀

▶

[Back](#)

[Close](#)

[Full Screen / Esc](#)

[Printer-friendly Version](#)

[Interactive Discussion](#)



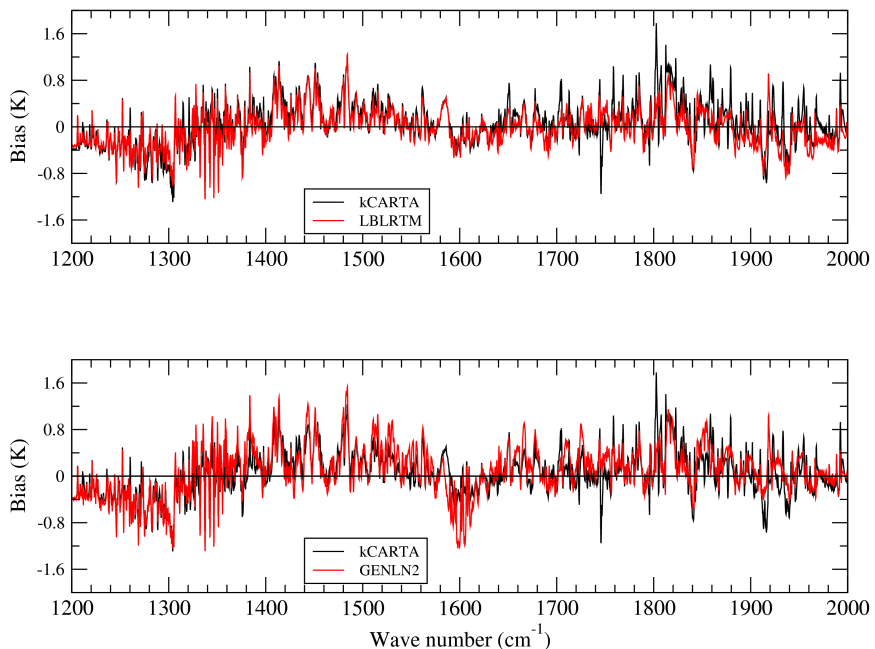


Fig. 10. The mean value of the difference between observed and computed brightness temperatures in the Southern Hemisphere for IASI band 2.

The accuracy of the RTTOV fast radiative transfer model

M. Matricardi

[Title Page](#)

[Abstract](#)

[Introduction](#)

[Conclusions](#)

[References](#)

[Tables](#)

[Figures](#)

◀

▶

[Back](#)

[Close](#)

[Full Screen / Esc](#)

[Printer-friendly Version](#)

[Interactive Discussion](#)



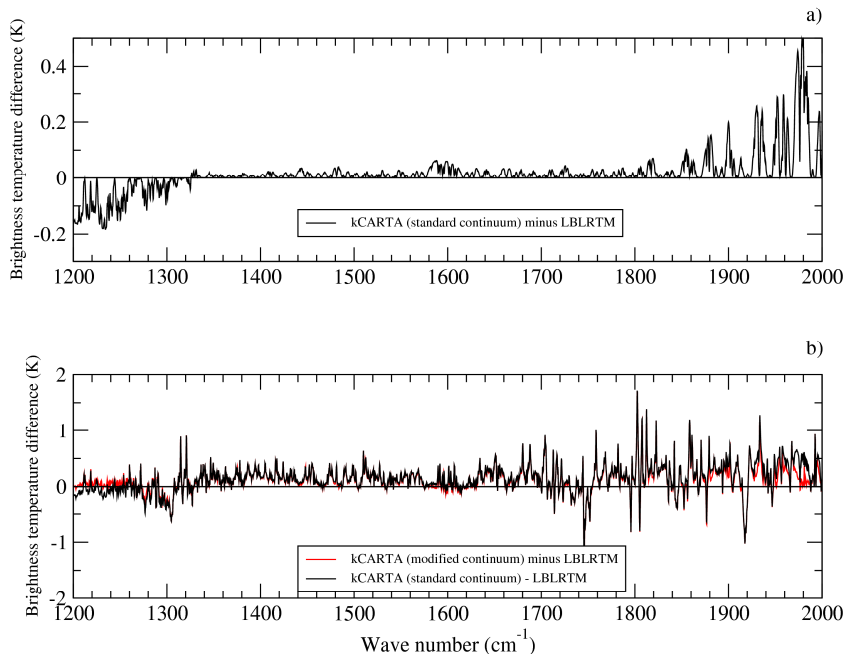


Fig. 11. The difference in the tropical region between (a) kCARTA and kCARTA_LBL; (b) kCARTA and LBLRTM (solid black line) and kCARTA_LBL and LBLRTM (solid red line).

The accuracy of the RTTOV fast radiative transfer model

M. Matricardi

[Title Page](#)

[Abstract](#)

[Introduction](#)

[Conclusions](#)

[References](#)

[Tables](#)

[Figures](#)

◀

▶

[Back](#)

[Close](#)

[Full Screen / Esc](#)

[Printer-friendly Version](#)

[Interactive Discussion](#)



The accuracy of the RTTOV fast radiative transfer model

M. Matricardi

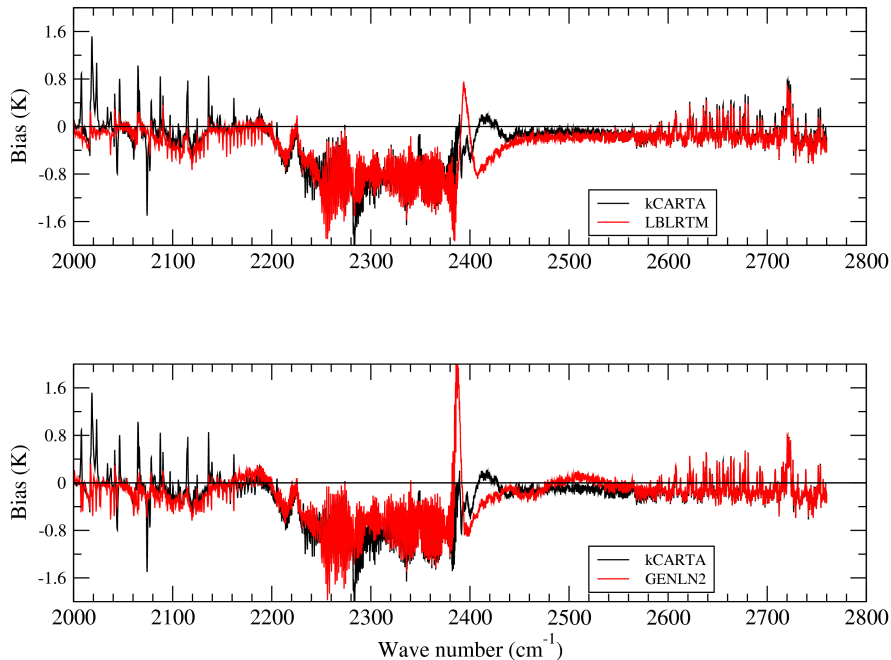


Fig. 12. the mean value of the difference between observed and computed brightness temperatures in the Northern Hemisphere for IASI band 3.

[Title Page](#)

[Abstract](#)

[Introduction](#)

[Conclusions](#)

[References](#)

[Tables](#)

[Figures](#)

◀

▶

[Back](#)

[Close](#)

[Full Screen / Esc](#)

[Printer-friendly Version](#)

[Interactive Discussion](#)

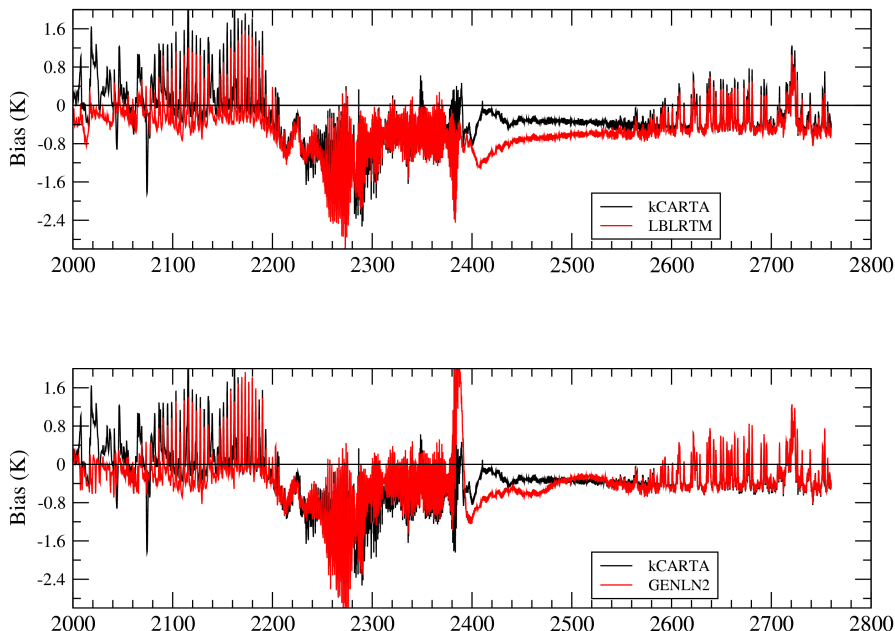


Fig. 13. The mean value of the difference between observed and computed brightness temperatures in the tropical region for IASI band 3.

The accuracy of the RTTOV fast radiative transfer model

M. Matricardi

[Title Page](#)

[Abstract](#)

[Introduction](#)

[Conclusions](#)

[References](#)

[Tables](#)

[Figures](#)

◀

▶

[Back](#)

[Close](#)

[Full Screen / Esc](#)

[Printer-friendly Version](#)

[Interactive Discussion](#)



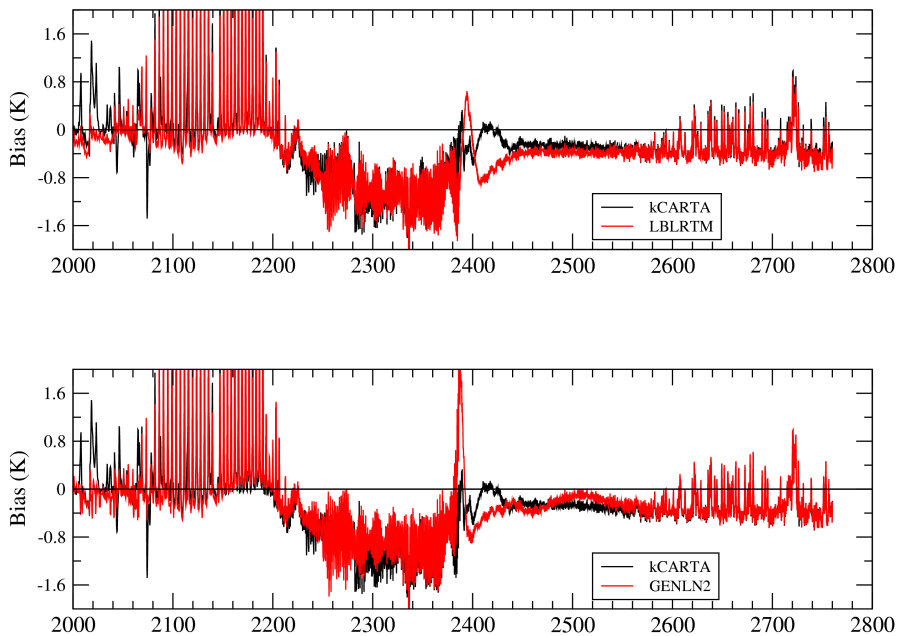


Fig. 14. The mean value of the difference between observed and computed brightness temperatures in the Southern Hemisphere for IASI band 3.

The accuracy of the RTTOV fast radiative transfer model

M. Matricardi

[Title Page](#)

[Abstract](#)

[Introduction](#)

[Conclusions](#)

[References](#)

[Tables](#)

[Figures](#)

[◀](#)

[▶](#)

[◀](#)

[▶](#)

[Close](#)

[Full Screen / Esc](#)

[Printer-friendly Version](#)

[Interactive Discussion](#)



The accuracy of the RTTOV fast radiative transfer model

M. Matricardi

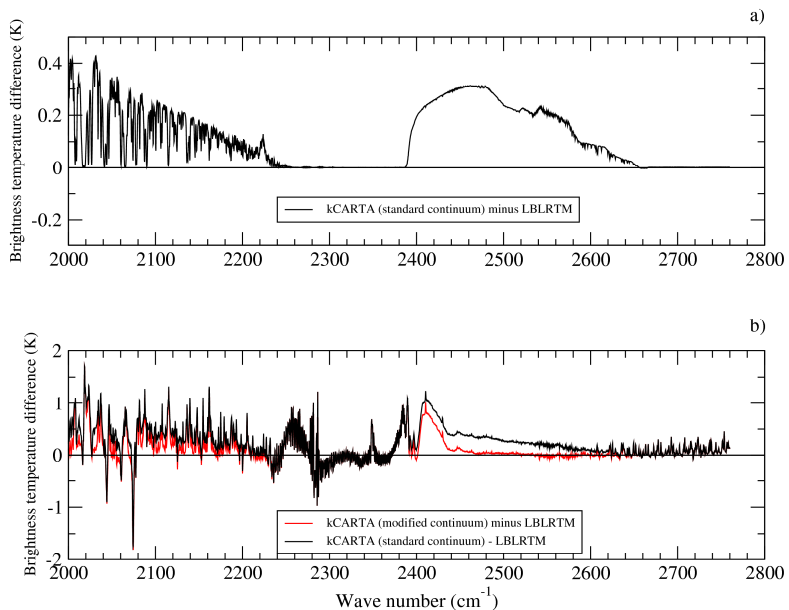


Fig. 15. The difference in the tropical region between **(a)** kCARTA and kCARTA_LBL; **(b)** kCARTA and LBLRTM (solid black line) and kCARTA_LBL and LBLRTM (solid red line).

[Title Page](#)

[Abstract](#)

[Introduction](#)

[Conclusions](#)

[References](#)

[Tables](#)

[Figures](#)

◀

▶

[Back](#)

[Close](#)

[Full Screen / Esc](#)

[Printer-friendly Version](#)

[Interactive Discussion](#)

